

On the mass and origin of Chariklo's rings

Margaret Pan (pan@astro.utoronto.ca), Yanqin Wu

Department of Astronomy & Astrophysics, 50 St. George Street, University of Toronto, Canada

ABSTRACT

Observations in 2013 and 2014 of the Centaur 10199 Chariklo and its ring system consistently indicated that the radial width of the inner, more massive ring varies with longitude. That strongly suggests that this ring has a finite eccentricity despite the fast differential precession that Chariklo's large quadrupole moment should induce. If the inferred apse alignment is maintained by the ring's self-gravity, as it is for the Uranian rings, we estimate a ring mass of a few times 10^{16} g and a typical particle size of a few meters. These imply a short collisional spreading time of $\sim 10^5$ years, somewhat shorter than the typical Centaur dynamical lifetime of a few Myrs and much shorter than the age of the solar system. In light of this time constraint, we evaluate previously suggested ring formation pathways including collisional ejection and satellite disruption. We also investigate in detail a contrasting formation mechanism, the lofting of dust particles off Chariklo's surface into orbit via outflows of sublimating CO and/or N₂ triggered after Chariklo was scattered inward by giant planets. This latter scenario predicts that rings should be common among 100-km class Centaurs but rare among Kuiper belt objects and smaller Centaurs. It also predicts that Centaurs should show seasonal variations in cometary activity with activity maxima occurring shortly after equinox.

1. Introduction

Occultation observations of the Centaur 10199 Chariklo on 2013 June 3 revealed two dense narrow rings, the first discovered around a minor planet (Braga-Ribas et al. 2014). This surprising announcement immediately raised questions about the formation, lifetime, and ubiquity of rings around small bodies with active dynamical histories: Centaurs are thought to be Kuiper belt objects (KBOs) scattered into the giant planet region by planetary encounters, and their typical dynamical lifetime is \sim few Myr (Bailey & Malhotra 2009).

The discovery observation resolved the inner and more massive¹ of the rings and, intriguingly, showed a significant difference between the ring widths measured during ingress (7.17 ± 0.14 km) and egress (6.16 ± 0.11 km). Further occultations in 2014 again indicated azimuthal variations in the

¹The outer ring, which Braga-Ribas et al. (2014) believe has about one-tenth the inner ring's mass, was only just resolved by the discovery occultation, and its width measurements are much less precise.

width of the inner ring (Sicardy et al. 2014). If these variations are long-lived, they strongly suggest an apse-aligned ring with a finite eccentricity spread and, therefore, a finite overall eccentricity (see, for example Nicholson et al. 1978). This apse-alignment is surprising since Chariklo’s large oblateness ($\varepsilon = 0.213$, Braga-Ribas et al. 2014) and implied J_2 moment should cause fast differential precession within the ring.

This feature provides us with a convenient way to measure the ring mass. Inspired by the work of Goldreich & Tremaine (1979b,a) on the narrow dense Uranian rings, we describe here a simple model of Chariklo’s inner ring in which Chariklo’s oblateness and the ring’s self-gravity together maintain the ring’s apse alignment. We apply this model to derive a mass, typical particle size, and collisional spreading time for the ring (§2). We discuss our results’ implications for existing dynamical/collisional ring formation models (§3), then propose and discuss a completely different model where the rings result from volatile outgassing (§4). Finally, we summarize our findings (§5).

2. Ring mass

2.1. Setup

Despite its small size (equatorial radius $R \sim 145$ km, Braga-Ribas et al. 2014), Chariklo appears quite oblate. Assuming circular rings whose center and orbit normal coincide with Chariklo’s center and axis of symmetry, Braga-Ribas et al. (2014) found an oblateness of $\varepsilon = 0.213 \pm 0.002$. Under the simplest assumption of uniform density, Chariklo’s lowest order gravitational moment would be $J_2 = \varepsilon(2 - \varepsilon)/5 \simeq 0.076$. If Chariklo has bulk density ~ 1 g cm⁻³, the implied differential precession timescale for a ring with semimajor axis $a \simeq 390$ km and radial width $\Delta a \simeq 7$ km (see Table 1) would be of order

$$\frac{1}{J_2} \frac{a^2}{R^2} \frac{a}{\Delta a} \frac{1}{\Omega} \simeq 17 \text{ months} \quad , \quad (1)$$

far shorter than any plausible system lifetime.

At the same time, multiple occultations in 2013 and 2014 indicate that the width of Chariklo’s inner, more massive ring varies with longitude from ~ 5.5 km to ~ 7.1 km (El Moutamid 2014; Sicardy et al. 2014). Given the short orbit period (~ 16.4 hrs), this strongly suggests an eccentric apse-aligned ring whose eccentricity varies by at least $\Delta e \sim \delta(\Delta a)/a \simeq (7.1 - 5.5)/390.6 \simeq 0.004$ over the ring’s total width. The mean eccentricity e must be at least Δe — in a similar context, the rings of Uranus have eccentricities 7 to 11 times larger than Δe (French et al. 1991).

To maintain apse alignment in Chariklo’s rings, other forces must counter the dispersive effects Chariklo’s J_2 . One possibility is self-gravity within the ring, originally suggested by Goldreich & Tremaine (1979a,b) to explain the apse alignment of the Uranian rings. To see this qualitatively, we think of the ring as a collection of non-crossing radially nested ringlets, a reasonable model for a cold system with frequent collisions; self-gravity causes outer ringlets to feel an inwards radial force while inner ringlets feel an outwards radial force. In an eccentric ring that is narrower at periapse than at

apoapse, the self-gravity forces at periapse dominate over those at other longitudes, so we can approximate these forces as impulses at periapse. Such forces tend to enhance the forward precession of the outer ringlets and slow that of the inner ringlets, cancelling the differential precession due to Chariklo’s quadrupole.

Given the observed system parameters, we can solve for the ring mass m needed to maintain apse alignment. We give an order of magnitude estimate here (ahead of an exact solution in §2.2) by dividing a narrow ring into just two apse-aligned ringlets of masses $m/2$, eccentricities e and $e + \Delta e$, where $0 < \Delta e \ll e \ll 1$, and semimajor axes a and $a + \Delta a$, where $\Delta a \ll a$. We find the total gravitational force between the ringlets by estimating the force at each point and summing over longitude. For a point on, say, the inner ringlet at true anomaly f , the force arises mostly from a segment of the outer ringlet at the same true anomaly at a distance $d \sim \Delta a(1 - q \cos f)$ away where

$$q = \frac{d(ae)}{da} \approx e + \frac{a\Delta e}{\Delta a} \sim a \frac{\Delta e}{\Delta a}. \quad (2)$$

Non-crossing orbits in a ring narrower at periapse than apoapse require $0 < q \leq 1$. Since $d \ll a$ we treat the segment on the outer ringlet as an infinite wire to find

$$\text{self-grav. accel.} \sim \frac{Gm}{\pi a \Delta a (1 - q \cos f)} + O(e^2) \quad . \quad (3)$$

This acceleration is mostly radial; the tangential component is smaller by a factor of order e . Lagrange’s equations (Murray & Dermott 1999) then give an orbit averaged precession rate of

$$\left. \frac{d\varpi}{dt} \right|_{\text{self}} \sim \int_{\text{ringlet}} df \frac{\cos f}{\Omega a e} \cdot \frac{Gm}{a \Delta a (1 - q \cos f)} \sim \frac{Gm}{a(\Delta a)^2 \Omega} \frac{\Delta e}{e}. \quad (4)$$

Setting this equal to the reciprocal of the right-hand side of equation 1 yields

$$m \sim M J_2 \frac{e}{\Delta e} \left(\frac{R}{a} \right)^2 \left(\frac{\Delta a}{a} \right)^3 \sim 5 \times 10^{15} \text{ g} \left(\frac{e/\Delta e}{10} \right) \quad . \quad (5)$$

where we assume Chariklo is an oblate spheroid with obliquity 0.213, constant bulk density $\rho = 1 \text{ g cm}^{-3}$ and total mass $M \simeq 10^{22} \text{ g}$. Note that finite e and Δe are crucial to the calculation of $d\varpi/dt|_{\text{self}}$.

2.2. Exact solution

Following the procedure of Goldreich & Tremaine (1979a), we divide a narrow apse-aligned eccentric ring into N ringlets and compute the interaction between ringlets j, k . Let ringlet j have semi-major axis a_j , eccentricity e_j , and fraction h_j of the total ring mass m . To lowest order in eccentricity, the force from ringlet k on a point on ringlet j is

$$\mathbf{F}_{\text{point}} = \frac{Gm h_k}{2\pi a_k (1 + e_k \cos f)} \frac{(\hat{\mathbf{r}} - \hat{\boldsymbol{\theta}} \sin f)}{(a_k - a_j)(1 - q_{jk} \cos f)}, \quad (6)$$

where $\hat{\mathbf{r}}$, $\hat{\boldsymbol{\theta}}$ are the radial and tangential unit vectors and

$$q_{jk} = \left. \frac{d(ae)}{da} \right|_{jk} \simeq \frac{a(e_k - e_j) + e(a_k - a_j)}{a_k - a_j} . \quad (7)$$

This force induces a precession rate (Murray & Dermott 1999)

$$\left. \frac{d\omega}{dt} \right|_{\text{point}} = \frac{1}{\Omega_j a_j e_j} \left(-\hat{\mathbf{r}} \cos f + \hat{\boldsymbol{\theta}} \sin f (2 - e_j \cos f) \right) \cdot \mathbf{F}_{\text{point}} , \quad (8)$$

so the precession rate of ringlet j due to ringlet k 's gravity is

$$\begin{aligned} \left. \frac{d\omega}{dt} \right|_{\text{self},jk} &= \int_{\text{ringlet } j} df \left. \frac{d\omega}{dt} \right|_{\text{point}} \\ &\simeq -\frac{1}{\pi} \frac{h_k m \Omega}{NM} \frac{a}{e} \frac{a_j - a}{a_k - a_j} \frac{q_{jk} \left(1 - \sqrt{1 - q_{jk}^2} \right)}{q_{jk}^2 \sqrt{1 - q_{jk}^2}} . \end{aligned} \quad (9)$$

Since the differential precession rate of ringlet j due to Chariklo's J_2 is

$$\left. \frac{d\omega}{dt} \right|_{J_2,j} \simeq \text{const} - \frac{21}{4} J_2 \frac{R^2}{a^2} \frac{a_j - a}{a} \Omega , \quad (10)$$

the condition that self-gravity be strong enough to maintain apse alignment against J_2 -induced differential precession is

$$P = \left. \frac{d\omega}{dt} \right|_{J_2,j} + \sum_{k \neq j} \left. \frac{d\omega}{dt} \right|_{\text{self},jk} , \quad 0 < j, k \leq N \quad (11)$$

$$= C_1 j + C_2 m \sum_{k \neq j} \frac{h_k}{k - j} \quad (12)$$

where P , the overall ring precession rate, is independent of j , and C_1 , C_2 are functions only of M , J_2 , a , Δa , e , Δe . In Eq. 12 we also take the ringlets to be evenly spaced in semimajor axis, $a_k - a_j = (k - j)\Delta a/N$, without loss of generality. With $e_1 = e$, $e_N = e + \Delta e$, and a choice for the ring density profile h_k , Eq. 12 gives N equations in the N unknowns P , m , e_2 , ..., e_{N-1} that in general have an exact solution.

2.3. Results

Because we have only a rough lower bound on Δe and e , we solved the system of Eq. 12 for a grid of values $0.06 \leq e \leq 0.17$, $0.003 \leq \Delta e \leq 0.0065$. By analogy to the Uranian system, we chose $e \gtrsim$ several times Δe . An N -dimensional Newton's method solver produced the ring masses in Figure 1 for constant and quadratic surface density profiles h_k . Further experiments with profiles of the form $h_k = Ak^p + B$ with p even, $0 \leq p \leq 16$ and A and B coefficients chosen to yield

Chariklo	Equatorial radius ¹	R	144.9 ± 0.2
	Oblateness ¹	ε	0.213
Inner ring	Radius ¹	a_1	390.6 ± 3.3
	Radial width ²	Δa_1	5.5 to 7.1
	Optical depth ¹	τ_1	0.449 ± 0.009 0.317 ± 0.008
Outer ring	Radius ¹	a_2	404.8 ± 3.3
	Radial width ¹	Δa_2	$3.6^{+1.3}_{-2.0}$
	Optical depth ¹	τ_2	$0.05^{+0.06}_{-0.01}$ $0.07^{+0.05}_{-0.03}$
Gap between the rings ¹			9.0 ± 0.4 8.3 ± 0.2

¹Braga-Ribas et al. (2014)

²Sicardy et al. (2014); El Moutamid (2014)

Table 1: Observed physical properties of 10199 Chariklo and its rings. All lengths are in kilometers. Where two values with uncertainties are listed, the first was measured from the ingress and the second from the egress portion of the 2013 June 3 occultation.

$0.1 \leq \max(h_k)/\min(h_k) \leq 10$, gave ring masses differing from those of Figure 1 by less than an order of magnitude. We performed similar experiments varying Chariklo’s shape and bulk density. Since the oblate spheroid shape found by Braga-Ribas et al. (2014) is somewhat uncertain, and since the rotation lightcurves of Fornasier et al. (2014a) suggest Chariklo may have an equatorial axis ratio of at least 1.1, we tried different J_2 values representing a Jacobi ellipsoid Chariklo with axis ratio 1.1 to 1.6 in the ring plane. Also, since densities for binary KBOs of sizes similar to Chariklo are typically 0.6 to 0.7 g cm⁻³ (see, for example, Grundy et al. 2015), we tried lowering our mass estimate for Chariklo to reflect these densities. These experiments together gave ring masses differing from those of Figure 1 by about a factor of two. This is reasonable: as equations 9-12 indicate, the ring mass is roughly proportional to Chariklo’s mass and J_2 moment, and these Jacobi ellipsoids have J_2 moments about twice that of the nominal oblate spheroid.

In short, our model predicts

$$\text{ring mass } m \simeq \text{few} \times 10^{16} \text{ g} \quad (13)$$

$$\text{average surface density } \sigma \simeq \text{few} \times 100 \text{ g cm}^{-2} \quad (14)$$

Assuming the ring particles collide frequently and form a monolayer — not unreasonable given the optical depth $\tau_1 \sim 0.32 - 0.45$ — we may also estimate

$$\text{typical particle size } s \simeq \text{few m} \quad (15)$$

$$\text{typical random velocity } v \simeq \text{mm/s} \quad (16)$$

The ring appears slightly gravitationally unstable with Toomre $Q \simeq$ a few tenths, and the particle size is coincidentally similar to that in Saturn’s C ring (Cuzzi et al. 2009).

We can also estimate a timescale for spreading due to collisional diffusion by noting the time between collisions is the orbit period divided by the optical depth, a typical collision changes a particle’s energy by a fraction $v/(\sqrt{3}\Omega a)$, and the potential energy spread across the ring is $\Delta a/a$. This gives

$$\text{radial spreading time} \sim \left(\frac{\Delta a/a}{v/(\sqrt{3}\Omega a)} \right)^2 \frac{1}{\tau_1} \frac{2\pi}{\Omega} \sim 10^5 \text{ years} \quad (17)$$

In the above we have neglected precession due to collisions within the ring since we believe that particle-particle collisions contribute much less than self-gravity to differential precession for the ring profiles we consider, in contrast to the situation in Uranus’s ϵ ring (Goldreich & Tremaine 1979a; Chiang & Goldreich 2000). While both J_2 and $\Delta a/a$ are much larger in the Chariklo system than in the Uranus system, the R/a and random velocity values are comparable. As a result, precession from the central body’s J_2 is much larger in the Chariklo system than in the Uranian case, while collisionally induced precession is much less important. However, if as in the work of Chiang & Goldreich (2000) on the Uranian system (a) shepherd satellite(s) increase(s) the random velocity by more than an order of magnitude near the edge(s) of Chariklo’s ring, collision-induced precession at the edge(s) may significantly affect the derived ring mass: to balance the

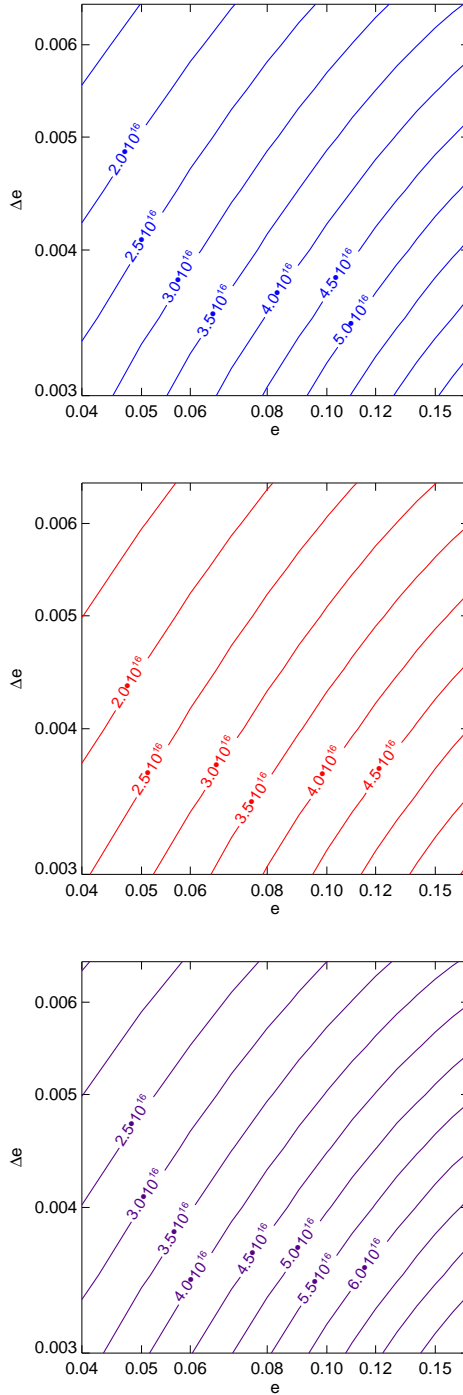


Fig. 1.— Contour plots of total ring mass in grams as a function of e , Δe for three possible ring surface density profiles: uniform, $h_k = 1/N$ (top); parabolic with edge densities half the value of the central density, $h_k = 3(j/N)^2 - 3j/N + 3/2$ (middle); parabolic with edge densities twice the value of the central density, $h_k = -12(j/N)^2/5 + 12(j/N)/5 + 9/5$ (bottom). The total mass increases by an order unity factor for profiles with mass concentrated towards ring edges.

collisional and J_2 terms in the Uranian rings, the total ring mass needs to increase by of order a factor of 10 (Chiang & Goldreich 2000).

Massive shepherd satellites could also significantly lengthen the spreading timescale. Confirming the existence of such (a) satellite(s) would require either an extremely high resolution ring profile or excellent luck in occultation timing. However, circumstantial evidence suggests that the satellite(s), if present, would be no larger than ~ 1 km in size. To be consistent with the width of the gap between Chariklo’s inner and outer rings, a shepherd in the gap would need to be ~ 1 km in size. Any shepherd interior to the rings must also be small. Since the rings are slightly gravitationally unstable, with Toomre $Q < 1$, they must lie within Chariklo’s Roche radius in order to avoid fragmentation.² An inner shepherd would likewise lie within the Roche radius. Since KBOs larger than ~ 300 km are expected to be rubble piles (see, for example, Stewart & Leinhardt 2009, and references therein), a large $\gtrsim 1$ km inner shepherd would likely be subject to tidal disruption. As the total ring mass is comparable to that of a 1-km body, a 1-km shepherd would slow collisional diffusion only by a factor of order unity³, at most mildly lengthening our estimate for the spreading time.

3. Constraints on dynamical formation scenarios

Recent reinterpretation of occultation data of the second-largest Centaur, 2060 Chiron, as possible evidence of rings (Ortiz et al. 2015; Ruprecht et al. 2015) has further sharpened interest in ways to form rings around small bodies which have had close encounters with giant planets. Dynamical formation mechanisms proposed thus far for Centaur ring systems (see, for example, Braga-Ribas et al. 2014; El Moutamid 2014; Duffard et al. 2014) fall into two broad categories which we discuss in light of our findings in §2.

3.1. Ejection

First, the rings may have formed while the Centaur was still a member of the Kuiper belt, probably via ejection of a small amount of material off the parent body’s surface into an orbit within the Roche radius. Cratering collisions are one way to do this. Simulations of such collisions at the ~ 1 km/s velocities typical of the Kuiper belt (see, for example, Leinhardt & Stewart 2012) indicate that the ejected mass is of order the impactor mass and that the vast majority of ejected material departs at speeds of order the escape velocity. Simulations of collisional satellite formation (see, for example, Canup 2004) likewise indicate that for velocities above the escape velocity, $< 1\%$

²Both shepherds and a Jacobi ellipsoid shape for Chariklo would decrease the Toomre Q further.

³A large > 1 km outer shepherd paired with a small inner shepherd would not slow diffusion significantly, as the ring would preferentially spread inward

of ejected material remains in orbit long-term. So most likely only a small fraction of the ejecta in any given collision with Chariklo (escape velocity $\sim 100 \text{ m s}^{-1}$) would remain in a close orbit. As the total mass of Chariklo’s rings is of order that of a $\sim 1 \text{ km}$ body, a ring creation event would require a substantially larger impactor which we take here to be $\sim 5 \text{ km}$.

From Schlichting et al. (2012), the optical depth to collisions for a $\sim 150\text{-km}$ target is $\sim 4.6 \times 10^{-8} [5 \text{ km/projectile size}]^{2.7}$, suggesting that a body like Chariklo would have collided with a $\sim 5\text{-km}$ projectile a few times over its few-Gyr residence time in the Kuiper belt. It therefore seems plausible that most KBOs of Chariklo’s size could acquire ring systems or at least small satellites in this way. However, the short $\sim 10^5\text{-year}$ ring spreading time we find in §2.3 suggests that such systems formed of order $\gtrsim 1 \text{ Gyr}$ ago would have dispersed to low optical depths by the present day.

Rotational disruption may also lift boulders from the surface into orbit; it may explain how near-Earth asteroids (see, for example, Descamps & Marchis 2008, and references therein) and in at least one case a KBO (Ortiz et al. 2012) shed material from their surfaces into orbit, creating small satellites. This mechanism seems less likely for Chariklo because its $\sim 7\text{-hr}$ spin period (Fornasier et al. 2014b) is not extremely close to breakup⁴, and because rotational disruption is infrequent enough that occurrence in the last 10^5 yrs is unlikely.

3.2. Satellite disruption

Second, the rings may have formed during the close encounter(s) with a giant planet, most likely Neptune, that brought the parent body from the Kuiper belt to a Centaur orbit. For example, this encounter may have perturbed a small moon inward the Roche radius, forcing it to tidally disrupt into a ring.

Such a moon may have been captured by dynamical friction in the early history of the Kuiper belt (Noll et al. 2008; Goldreich et al. 2002). Moons of this kind tend to have close orbits and be similar in mass to the central body. Alternatively, as discussed above, a typical $\sim 150\text{-km}$ KBO today has collided with a $\sim 5 \text{ km}$ projectile, placing perhaps $\lesssim 1\%$ of the projectile mass into orbit. If these ejecta end up outside the Roche radius, they may well coalesce into satellites as described by Canup (2004) for the Earth-Moon system and hypothesized for the small moons observed around large KBOs (Brown et al. 2006).

The tidal force needed to perturb a satellite inside the KBO’s Roche radius during a Neptune close encounter depends on the satellite’s initial orbit. We consider the case where the semimajor axes of the initial satellite orbit and the final ring differ by a factor of order unity and justify below why this is the most probable scenario. If the satellite’s initial semimajor axis is a_0 , the change

⁴Some binary asteroids that are believed to have formed via rotational fission do rotate slowly (see, for example Pravec et al. 2010). This occurs when the secondary is massive enough to convert rotational energy of the primary into its orbital energy.

in velocity produced by the tidal force during a single Neptune encounter with closest approach distance b is

$$\frac{GM_{\text{Neptune}}}{b^2} \frac{2a_0}{b} \frac{b}{u}, \quad (18)$$

where u is the typical random velocity of a Neptune-crossing KBO. To change the semimajor axis by a factor of order unity, this velocity change must be of order the ring orbit velocity $\sqrt{GM/a_1} = \Omega a_1$, implying

$$b \sim \sqrt{\frac{2GM_{\text{Neptune}}}{u\Omega}} \sqrt{\frac{a_0}{a_1}} \sim 3.6 \times 10^{10} \text{ cm} \sqrt{\frac{a_0/a_1}{2}} \sim 15 R_{\text{Neptune}}, \quad (19)$$

where we use $u \simeq 2$ km/s. For this encounter, the impact parameter at infinity is $b_\infty \sim b\sqrt{GM_{\text{Neptune}}/b}/u \sim 7.8 \times 10^{10}$ cm. The same encounter changes the KBO's solar orbital velocity by of order $GM_{\text{Neptune}}/(b_\infty u) \sim 4.4$ km/s, which is just enough to move the KBO onto a Centaur orbit. The Centaur creation event may thus also serve as a ring creation event.

Note that this scenario works only for KBOs that attain Centaur orbits via a single close Neptune encounter rather than multiple weak encounters. The much longer encounter duration in a weak scattering means the satellite can complete many orbits during a single encounter, severely diluting the effect of the tidal force. As a result, the KBO will likely become a Centaur before the moon's orbit changes significantly. At the same time, a single very close Neptune encounter that changes the moon's orbit velocity by more than an order unity factor will most likely unbind the moon from the KBO. Ring formation via satellite disruption thus requires a single Neptune encounter and a close match between the satellite orbit and the Neptune encounter strength.

This condition allows us to estimate the frequency of such satellite disruptions. Since the number of Centaurs created scales logarithmically with the distance of the closest encounter, and there are about 6 natural logarithmic intervals between $10R_{\text{Neptune}}$ and Neptune's Hill radius, we expect that about one in six Centaurs formed via a single Neptune encounter. The typical Centaur dynamical lifetime of \sim few million years (Bailey & Malhotra 2009) and the $\sim 10^5$ -year ring spreading time suggests that only a small fraction of these, $\sim 10\%$, would remain visible today. In the best scenario — i.e. if every large KBO has a close-in satellite, and assuming the single encounter with Neptune is just strong enough for the KBO to attain a Centaur-class orbit — the chance of observing a Centaur with rings is \sim few percent.

A further difficulty is the rapid rate of collisional destruction of small moons. At an impact velocity of ~ 1 km/s, the typical random velocity in the Kuiper belt, a ~ 20 m impactor can destroy a ~ 1 km moon. Assuming a size distribution consistent with Schlichting et al. (2012), the rate at which a given 1 km target encounters 20 m impactors in the current Kuiper belt is about once every 10^5 years, far faster than the creation rate of 1 km moons by impacts as described in §3.1 above. Rotational fission is likewise unlikely to create moons fast enough to beat collisional destruction.

The fast collisional destruction rate also makes significant collisional perturbation of a moon's orbit difficult. While a projectile of size at least \sim few hundred meters is needed to change the momentum of a 1 km moon by a factor of order unity, such a collision is likely to occur only once

every \sim Gyr. Even assuming the moon’s orbit is just a factor of ~ 2 larger than the Roche radius, the moon will be destroyed before it can be collisionally moved close enough to the Centaur.

For satellite disruption to be viable for ring formation at all, the satellites must therefore be more massive than the observed ring. Since the catastrophic collision timescale for a 10- to 20-km KBO is about a Gyr, a moon of that size could plausibly survive until Centaur orbit insertion. The fraction of ~ 100 -km KBOs with moons of this size is unknown: these moons are too large to form efficiently via cratering impacts and too small to be captured efficiently via dynamical friction, though rotational fission may provide an effective pathway. Nevertheless, moons of similar size have been found around a few of the largest KBOs (Ragozzine & Brown 2009; Brozović et al. 2015). Tidal disruption of such a large moon inside the Roche radius would lead initially to a much more massive disk/ring, but because the initial diffusive spreading time would be correspondingly shorter, the ring lifetime would not be significantly longer than our estimate in §2.3 above.

We conclude that among dynamical channels, compatibility between the ring spreading timescale and the expected time since formation weakly favors formation during a Neptune close encounter, not during the few-Gyr residence time in the Kuiper belt. However, this scenario requires that most ~ 100 -km KBOs have moons of size tens of kilometers or more, and it predicts a Centaur ring occurrence rate of at most a few percent.

4. Ring formation via outgassing

In view of the uncertainties in the dynamical formation channels discussed in §3, we develop a contrasting mechanism for ring formation, dusty outgassing, briefly alluded to by Braga-Ribas et al. (2014). Specifically, we discuss a simple model in which a dusty outflow entrained by CO sublimating within Chariklo deposits particles in close orbits. In §4.3, we collect the available Centaur observations and discuss them in the context of our theoretical predictions.

4.1. Chariklo’s history of CO loss

We first estimate the rate and velocity of CO outgassing from Chariklo, taking into account its dynamical history. We focus on CO here because of its high abundance and physical-chemical properties, but most of the discussion below applies if another volatile gas e.g. N_2 , CO_2 , CN, is substituted. In particular, N_2 has properties very similar to CO in both triple point temperature and saturation vapor pressure and may be more abundant.

We do not consider the alternative outgassing model where volatile gases are released by the exothermic process of water ice crystallization. While this process would increase the mass-loss rate above our estimates, we believe the correction would be order unity or less: scaling the crystallization model for Chiron (Priyalnik et al. 1995) to the distance of Chariklo gives an outgassing

rate comparable to or smaller than ours.

4.1.1. CO free escape vs. diffusion

As previous works have noted (see, for example, Cowan & Ahearn 1982; Jewitt 2009), sublimation of surface CO is fast even for bodies in the Kuiper belt. An estimate of the maximum sublimation rate follows from equating the rates of insolation and latent heat absorption:

$$\begin{aligned} \dot{m}_{\text{CO,max}} &\leq \frac{1}{E_{\text{latent}}} \frac{(1-A)L_{\odot}}{4\pi a^2} \frac{\pi R^2}{4\pi R^2} \\ &\sim 5.3 \times 10^{-7} \text{ g/s/cm}^2 \left(\frac{a}{16 \text{ AU}} \right)^{-2}, \end{aligned} \quad (20)$$

where the latent heat of CO sublimation is $E_{\text{latent}} \sim 240\text{J/g}$, the albedo is taken to be $A \sim 0.04$ (Fornasier et al. 2014b), and a is Chariklo’s semimajor axis in its orbit around the sun. Including surface cooling introduces only a small correction (Cowan & Ahearn 1982; Jewitt 2009). At this rate, assuming a CO mass fraction $f_{\text{CO}} \simeq 0.10$ (in line with previous comet measurements in e.g. Cochran et al. 2015), Chariklo would have outgassed all of its CO in 10^5 yrs in the Kuiper belt (also see Jewitt 2009), well before being scattered inward.

However, as numerous works have also argued (e.g., Enzian et al. 1997; De Sanctis et al. 2001; Guilbert-Lepoutre 2011), this rate applies only to CO that is exposed on the surface and can escape freely. If CO is instead interspersed with ice and dust grains throughout the body, then once the surface CO departs, the CO vapor must first diffuse upward through the ice/dust matrix in order to escape⁵ and the loss rate slows significantly.

To estimate this slower loss rate, we consider the upward diffusion of a CO molecule through convoluted tunnels formed by loosely packed icy/dusty grains.⁶ Let the average size and number density of grains be s and n respectively. The porosity of the medium is then $\phi = 1 - n4\pi/3s^3$ and the mean free path for gas-grain collisions is $l_{\text{mfp}} \sim 1/n\pi s^2 \sim s/(1-\phi)$. Assume solid CO remains only below a depth $\Delta\ell$. The CO vapor pressure is the saturated value $p_v = p_v(T)$ at this depth and decreases upward. The diffusive mass flux driven by the vapor density gradient over a single tunnel is

$$J \sim \pi s^2 D \frac{d}{dr} \rho_v \sim \pi s^2 D \frac{p_v(T)}{c_s^2 \Delta\ell}, \quad (21)$$

where we have assumed the typical tunnel cross section is πs^2 , the entire body has temperature T , c_s is the ideal gas sound speed at p_v and T , the vapor mass density is ρ_v , and the diffusion

⁵In principle, wherever the vapor pressure exceeds the tensile strength of the porous grains, vents can open and reexpose CO. However, even with the tensile strength $\sim 10^4$ dyne/cm² measured from tidal splitting of comets and lab simulations of cometary ice (Donn 1963; Whipple 1989; Kochan et al. 1989), the CO vapor pressure (see Fig. 2) is too low to form vents at any significant depth.

⁶The vapor density is so low that gas-gas collisions are irrelevant and the so-called ‘Knudsen regime’ applies.

coefficient is (Evans et al. 1961)

$$D \sim \frac{\phi}{\tau} l_{\text{mfp}} c_s \sim \frac{\phi}{\tau} \frac{s}{1-\phi} c_s, \quad (22)$$

where τ , the so-called tortuosity, covers our ignorance on factors such as the extended length of a tunnel due to topology, the width distribution among tunnels, and the scattering property of gas molecules off the tunnel wall. Over a unit surface area containing $\sim 1/(\pi s^2)$ tunnels, the total mass-loss rate is

$$\dot{m}_{\text{CO}} \sim \frac{1}{\pi s^2} J \sim \frac{\phi}{\tau} \frac{s}{1-\phi} \frac{p_v(T)}{c_s \Delta \ell}. \quad (23)$$

To determine the appropriate depletion depth $\Delta \ell$, also called the sublimation front, we assume that Chariklo has been outgassing at temperature T for most of its lifetime t_{age} ,

$$\dot{m}_{\text{CO}} \times t_{\text{age}} = \Delta \ell \times \rho \times f_{\text{CO}}. \quad (24)$$

We take the saturation vapor pressure to be (Clayton & Giauque 1932)

$$p_v(T) \simeq 0.15 \text{ bar} \exp \left[6.15 \left(1 - \frac{68 \text{ K}}{T} \right) \right], \quad (25)$$

where the temperature is the local blackbody value at distance a , that is, $T = T_{\text{BB}}$ where

$$\sigma_{\text{SB}} T_{\text{BB}}^4 = \frac{(1-A)L_{\odot}}{16\pi a^2}. \quad (26)$$

This assumes that the heat needed for sublimation is negligible compared to re-radiation (as we easily verified). The CO loss rates from this simple model, shown as red dots in Fig. 2, are orders of magnitude below the free escape loss rates (solid lines). In particular, in the \sim few Gyr that Chariklo presumably spent at 40 AU, the CO sublimation front would reach a depth 1 km (also see De Sanctis et al. 2001).⁷ If Chariklo had instead spent that time at 20 AU, all its CO would have been depleted.

Interestingly, we reach nearly identical conclusions if we substitute N_2 for CO in the above discussion. This suggests that evaporation of CO or N_2 , or both, can drive dusty outgassing. In contrast, CH_4 and CO_2 are unimportant here due to their much higher triple point temperatures.

4.1.2. *Becoming a Centaur*

Chariklo’s arrival in its current orbit ($a = 15.8$ AU) \sim few Myrs ago (Bailey & Malhotra 2009) should have strongly increased its temperature and CO loss rate, as we discuss below (also see De Sanctis et al. 2000).

⁷The limited loss of CO during the KBO stage also explains why objects like comets 29P/SW1 and comet Hale-Bopp showed CO outgassing. See §4.1.2.

While the surface temperature would have jumped immediately from ~ 41 K to 68 K once Chariklo reached 15.8 AU, the CO vapor pressure would have remained low until the CO-rich matrix at depth $\Delta\ell \simeq 1$ km also warmed. To estimate the heat diffusion time through $\Delta\ell$, we take the thermal conductivity to be $\kappa \sim 0.1$ W m $^{-1}$ K $^{-1}$, appropriate for a dust-ice aggregate (Enzian et al. 1997; De Sanctis et al. 2001; Guilbert-Lepoutre 2011), and we use specific heat capacity $c_p \sim 6 \times 10^6$ erg g $^{-1}$ K $^{-1}$ for an ice-dominated mixture between 40 and 70 Kelvin (Klinger 1980). The thermal diffusivity is then $\nu = \kappa/\rho c_p \sim 10^{-3}$ cm 2 s $^{-1}$, so the CO-rich interior should have stayed cold for ~ 1 Myr after Centaur orbit insertion. After this delay, the CO vapor pressure in the interior would have increased by a factor of $\sim 10^4$ (eq. 25). The CO diffusion rate would likewise have increased (eq. 23) from the original 10^{-13} g s $^{-1}$ cm $^{-2}$ to $\sim 10^{-9}$ g s $^{-1}$ cm $^{-2}$, or a global rate of 10^7 g s $^{-1}$ (also see Fig. 3).⁸ These jumps are shown as blue arrows in Fig. 2. The energy needed to maintain the new rate is negligible compared to insolation, consistent with our assumption in §4.1.1. Note that due to the sudden transition, this rate is higher than the equilibrium rate, i.e. the rate we would expect if Chariklo had remained at its current location for a few Gyrs.

We now estimate the total CO mass sublimated. Thermal diffusion limits the CO mass lost in Chariklo’s time as a Centaur: since $D > \nu$, new CO vapor can escape sufficiently fast and the thermal diffusion and CO sublimation fronts should nearly coincide. After 10 Myr, the thermal diffusion front lies ~ 5 km below the surface, and the total CO lost is

$$\Delta m_{\text{CO}} \sim \rho f_{\text{CO}} \times 5 \text{ km} \times 4\pi R^2 \sim 5 \times 10^{19} \text{ g}. \quad (27)$$

This is a few orders of magnitude higher than the ring mass we inferred, so the total CO outgassed is potentially enough to lift a ring’s worth of solids off the surface.

4.1.3. The “spring thaw”

Since neither of the pole solutions published by Braga-Ribas et al. (2014) coincide with Chariklo’s orbit normal, we expect strong seasonal variations in solar insolation. We now estimate the corresponding variations in CO outgassing for later reference in §4.2-4.3. In Chariklo’s polar regions the insolation variations cause large temperature fluctuations to a depth of order $d \sim \sqrt{P_{\text{orb}}\nu} \sim 10$ m, where $P_{\text{orb}} = 62$ yrs is Chariklo’s orbit period.⁹ The CO diffusing through this layer experiences freeze-thaw cycles that drastically modulate the surface outgassing rate.

Because CO spends $d^2/D \sim 2 \times 10^6$ s passing through this layer, its volume density there is $\rho_{\text{CO}} \sim \dot{m}_{\text{CO}} \times (d^2/D)/d \sim 10^{-6}$ g cm $^{-3}$ ($\dot{m}_{\text{CO}}/10^{-9}$), equivalent to a vapor pressure of $p \sim 2 \times 10^2$ dyne cm $^{-2}$. This is the saturation vapor pressure at ~ 47 K (eq. 25), so if the winter

⁸This is far above the result of De Sanctis et al. (2000) for a similar object. We suspect the difference arises because their integration is too short to allow the interior to thermalize.

⁹Chariklo’s small eccentricity has little impact on temperature.

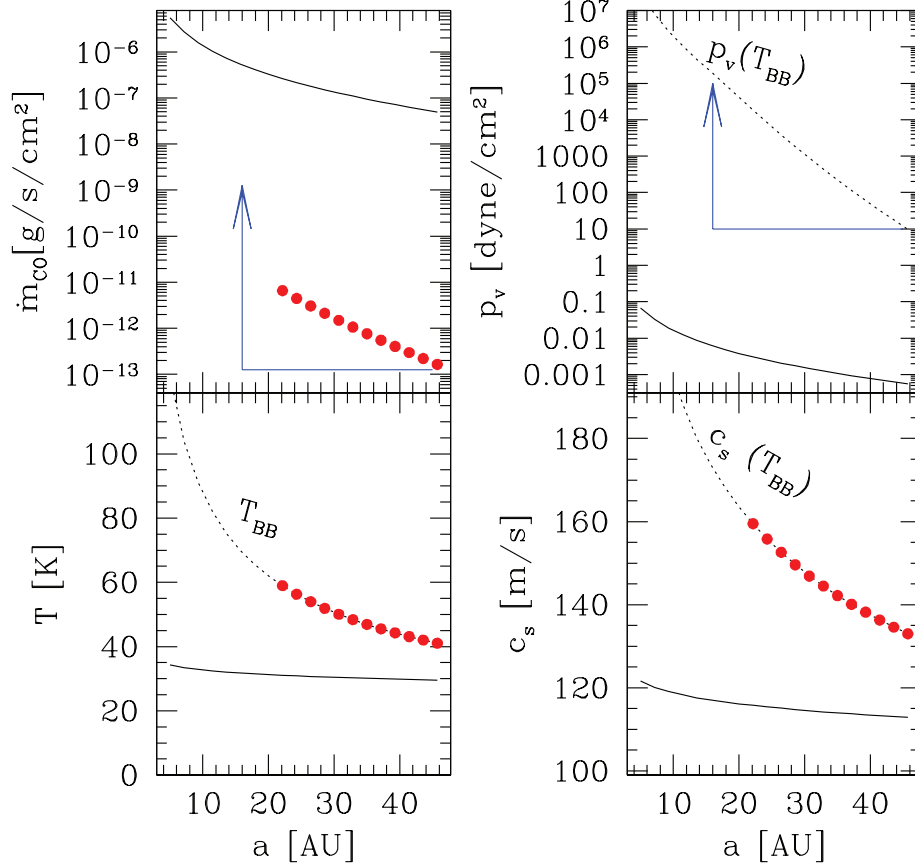


Fig. 2.— Comparison of (top left) CO outgassing rate, (bottom left) temperature, (top right) CO saturation vapor pressure, and (bottom right) sound speed under three different models. The black solid curves show conditions when CO is exposed on and sublimating directly from Chariklo’s surface (Eq. 20). In this model, most of the solar insolation is channelled into latent heat and the body maintains a temperature lower than the local blackbody value (black dotted curves marked T_{BB}). The red dots show conditions when surface CO is absent and CO loss occurs only through upward diffusion through an ice/dust matrix (Eq. 23). In this model, Chariklo stays close to the local blackbody temperature. For the computations we use bulk density $\rho = 1 \text{ g cm}^{-3}$, grain size $s = 1 \mu\text{m}$, porosity $\phi = 0.5$, tortuosity $\tau = 2$, $t_{\text{age}} = 4.5 \text{ Gyr}$ and present only results where the depletion length $\Delta\ell$ has not yet reached Chariklo’s center. The blue arrows indicate the increases in pressure and CO mass loss when Chariklo abruptly moved from 40 AU to 16 AU on becoming a Centaur. Seasonal freeze-thaw cycles can cause local outbursts whose outgassing rates greatly exceed the mass-loss rate at the tip of the blue arrow.

hemisphere cools below this point, CO will recondense. We can estimate the winter temperature by assuming that all heat content stored in layer d is radiated as blackbody radiation during the winter¹⁰:

$$d \times c_p \rho_{\text{CO}} (T_{\text{BB}} - T_{\text{winter}}) = \sigma T_{\text{winter}}^4 \times \frac{P_{\text{orb}}}{2} \longrightarrow T_{\text{winter}} \sim 38 \text{ K}. \quad (28)$$

Within the winter polar circle, CO therefore re-freezes on its way up from the deeper warm layer instead of escaping; in one winter $\dot{m}_{\text{CO}} \times P_{\text{orb}}/2 \sim 1 \text{ g/cm}^2$ accumulates, mostly in the coldest layers near the surface. When spring arrives, the sublimation and escape of this trapped CO proceeds nearly as for exposed CO (solid lines in Fig. 2), limited only by the insolation energy budget (Eq. 20). As this maximum rate, $\dot{m}_{\text{CO,max}} \simeq 5 \times 10^{-7} \text{ g/s/cm}^2$, is one or two orders of magnitude higher than the annual rate, the trapped surface CO is exhausted within a small fraction of an orbit. By assuming that the average annual CO loss is outgassed at the maximum rate, we estimate the minimum duration of such an outburst is ~ 50 days. The true duration is likely longer. Such short outgassing outbursts, occurring twice an orbit after equinoxes but not necessarily near periape, may have been seen in the 2-D simulations of Enzian et al. (1997).

4.2. Dust lifting and ring formation

Although the total CO lost is large compared to our ring mass of $\sim 10^{16}$ g, that does not guarantee that the momentum and energy of the CO outflow are enough to entrain dust particles and lift them into orbit. The minimum flow rate needed to lift a grain of size s_{dust} off the surface of Chariklo is

$$\frac{\rho_{\text{dust}} \frac{4\pi}{3} s_{\text{dust}}^3 \frac{GM}{R^2}}{\pi s_{\text{dust}}^2 c_s} \sim 2 \times 10^{-8} \text{ g cm}^{-2} \text{ s}^{-1} \\ \times \left(\frac{s_{\text{dust}}}{1 \mu\text{m}} \right) \left(\frac{170 \text{ m s}^{-1}}{c_s} \right) \left(\frac{R}{120 \text{ km}} \right) \left(\frac{\rho}{0.5 \text{ g cm}^{-3}} \right), \quad (29)$$

where we have adopted a dust grain density of $\rho_{\text{dust}} = 1 \text{ g cm}^{-3}$. While this assumes the gas-dust coupling is in the Stokes regime, the large mean free path we expect in the tenuous CO flow would reduce the drag by of order unity and increase the minimum required CO outflow rate by a similar factor.

The average gas outflow rate of $10^{-9} \text{ g cm}^{-2} \text{ s}^{-1}$ that we estimate in § 4.1.2 for a newly migrated Chariklo is thus unlikely to produce a dusty coma. This is consistent with Chariklo’s observed inactivity (Fornasier et al. 2014b). However, our discussion of the seasonal CO freeze/thaw suggests that in its current location, Chariklo could show short bursts of activity with regional mass outflows exceeding the constraint in Eq. (29).¹¹ At these times, we expect the CO vapor to approximately

¹⁰The latent heat released by CO condensing at a rate 10^{-9} g/s/cm^2 is negligible.

¹¹The recent detection of diurnal cycle of water ice sublimation on Comet 67P (De Sanctis et al. 2015) is an exact analogy of this time-dependent process, but happens on the diurnal timescale.

share its momentum with any entrained grains, accelerating them to a final speed

$$v_{\text{dust}} \sim \frac{c_s}{1+f} \simeq \frac{170 \text{ m s}^{-1}}{1+f} \left(\frac{T}{68 \text{ K}} \right)^{1/2} \quad (30)$$

where f is the solid to gas mass ratio in the outflow. If the dust and CO mass fractions are comparable, most dust grains will not attain the escape velocity of ~ 100 m/s — they remain bound to Chariklo. Indeed, Meech & Belton (1990) reached a similar conclusion for Chiron, a slightly smaller Centaur, arguing that predominantly bound grains may explain why Chiron’s coma has a steep surface-brightness profile more consistent with an atmosphere than an unbound halo.

Initially the outflow puts grains on roughly radial trajectories that re-intersect Chariklo’s surface within less than an orbit. Though Chariklo’s rotation (7-hr period; Fornasier et al. 2014b) imparts to the grains a tangential velocity of \sim one-third the surface escape speed (for a bulk density of 1 g cm^{-3}), this is only a fraction $\simeq 0.3 (7 \text{ hrs}/P_{\text{rot}}) (390 \text{ km}/a_1)^{1/2} (\rho/(1 \text{ g cm}^{-3}))^{-1/4}$ of the orbital angular momentum at distance a_1 . Grains will therefore quickly re-accrete onto Chariklo unless they collide with other grains before re-intercepting the surface. We can estimate the collision probability as follows. The mean-free path of grains in the outflow is $l_{\text{mfp}} \sim 1/n_{\text{dust}} \pi s_{\text{dust}}^2$, where grain number density $n_{\text{dust}} = f \dot{m}_{\text{CO}}/v_{\text{dust}}/(4\pi/3s^3 \rho_{\text{dust}})$. After a free-fall time $(1/\sqrt{G\rho})$, the collision probability is

$$\begin{aligned} \tau_{\text{collision}} &\sim \frac{t_{\text{dyn}}}{l_{\text{mfp}}/v_{\text{dust}}} \\ &\sim 5 \left(\frac{f \dot{m}_{\text{CO}}}{10^{-7} \text{ g cm}^{-2} \text{ s}^{-1}} \right) \left(\frac{0.5 \text{ g cm}^{-3}}{\rho} \right)^{1/2} \left(\frac{1 \mu\text{m}}{s} \right), \end{aligned} \quad (31)$$

Each grain should suffer multiple collisions given our estimated flow rate.¹²

We expect collisions to tend to redistribute angular momentum among grains, allowing a fraction ϵ_2 of the grains to remain in orbit. ϵ_2 is hard to estimate as it depends on the detailed collision geometry and collision probability. However, these surviving grains’ final orbits are most likely close to the surface, where collisions are more frequent and the required angular momentum is lower. Finally, grains that remain in orbit collide with one another, damping their relative velocities. Since the grains inherit Chariklo’s rotational velocity when they leave the surface, their total angular momentum is parallel to Chariklo’s. The grains’ mutual collisions cause them to settle into Chariklo’s equatorial plane in a ring configuration. This mechanism thus favors the formation of a ring that lies inward of the Roche radius, though close-in moons slightly further away are also possible. How these orbiting grains might attain the narrow dense ring geometry currently observed around Chariklo is not clear, however.

¹²Also, once an optically thick ring forms, it should accrete grains efficiently.

We can estimate the dust mass remaining in orbit as

$$m_{\text{ring}} \approx f \epsilon_1 \epsilon_2 \Delta m_{\text{CO}} \sim 5 \times 10^{16} \text{ g} \\ \times \left(\frac{f}{1}\right) \left(\frac{\epsilon_1}{0.1}\right) \left(\frac{\epsilon_2}{10^{-2}}\right) \left(\frac{\Delta m_{\text{CO}}}{5 \times 10^{19} \text{ g}}\right). \quad (32)$$

Here ϵ_1 is the fraction of the CO loss that occurs in short outbursts — roughly, the fractional area of polar regions on Chariklo multiplied by the fractional length of winter. When the obliquity is 90 deg, $\epsilon_1 \sim 0.25$; the pole solutions of Braga-Ribas et al. (2014) and the orbit given for Chariklo in the JPL Small Body Database indicate the polar regions cover about one-half the total surface, so we adopt $\epsilon_1 \sim 0.1$. While ϵ_2 is highly uncertain, unless $\epsilon_2 \ll 10^{-2}$ the dust mass placed in orbit via CO outgassing is comparable to our calculations in §2, which is encouraging.

The particle size of ~few meters we estimate for the current ring is likely unrelated to the original grain size. Frequent collisions may cause the grains to stick together mechanically, increasing the typical particle size. We leave a detailed description of ring particle growth, and of the particles’ settling into a narrow ring geometry, to future work.

4.3. Confronting Observations

We now collect available observations on Centaurs to test two important aspects of our model: 1) that CO should be preserved in the deep interior and may sublime and diffusively migrate to the surface once the Centaurs are heated in their new location; and 2) that CO outgassing may lift dust grains off their surfaces either continuously for hotter Centaurs or upon the start of spring in colder Centaurs.

Highly relevant for the first of these are observations of comet outgassing, which suggest that CO (and possibly CO₂) is relatively abundant (~10% relative to H₂O, Cochran et al. 2015), while O₂ occurs at a surprisingly high ~3% (Bieler et al. 2015; Rubin et al. 2015b) and N₂ occurs at a surprisingly low ~0.1% (Rubin et al. 2015a). This motivates us to focus on CO. We argue in §4.1.1 that while exposed CO on KBO surfaces would have sublimated long ago, CO should retain its primordial abundance in layers deeper than ~1 km and could diffuse upward rapidly upon displacement of the KBOs to warmer regions of the solar system. This may explain the detection of CO outgassing in Comet 29P/SW1 ($a = 6$ AU, $R \sim 15$ km, Senay & Jewitt 1994; Crovisier et al. 1995; Gunnarsson et al. 2002), Comet Hale-Bopp (at $a \sim 7$ AU, $R \sim 20$ km, Biver et al. 1997), and possibly Centaur 2060 Chiron ($a = 13.7$ AU, $R \sim 100$ km, Womack & Stern (1997), though this has been challenged by Rauer et al. (1997); Bockelée-Morvan et al. (2001)). For these objects our simple model predicts CO loss rates between $10^{-7} \text{ g cm}^{-2} \text{ s}^{-1}$ and $10^{-9} \text{ g cm}^{-2} \text{ s}^{-1}$, depending on their current orbits, consistent with observations. But our explanation is not unique (e.g. Prialnik & Bar-Nun 1987), and a number of surveys (Rauer et al. 1997; Bockelée-Morvan et al. 2001; Jewitt et al. 2008) have failed to detect CO around other Centaurs and KBOs. Some of these upper limits contradict our predictions (Fig. 3): for the few largest Centaurs like Chariklo, Chiron,

Pholus and Asbolus, we predict outgassing rates some 1-2 orders of magnitude above the observed upper limits. This could be partly due to a residence time in the Centaur region of \gtrsim few Myr, since CO outgassing slows as the sublimation front retreats further below the surface.

For information on dust grain lifting we turn to observations of cometary activity in Centaurs (Jewitt 2009). The origin of these cold objects’ activity remains a puzzle. Jewitt (2009) has argued that CO outgassing cannot be the correct explanation based on the simple $1/r^2$ law expected for surface CO sublimation rate. However, as our calculation in Fig. 4 shows, our predicted CO outgas rates largely explains the observed dust production rates in active Centaurs. The outgas rate depends almost exponentially (not as $1/r^2$) on the illumination-weighted orbital separation, which in turn depends on the semimajor axis and the eccentricity. Moreover, for all but one of the Centaurs observed to be active we predict $\dot{m}_{\text{CO}} \gtrsim 10^{-8} \text{ g cm}^{-2} \text{ s}^{-1}$, the criterion for dust lifting in Eq. (29). Similarly, most Centaurs observed to be inactive have predicted CO outgas rates below $10^{-8} \text{ g cm}^{-2} \text{ s}^{-1}$, though a handful of inactive objects with high predicted CO outgas rates exist.

For Chariklo we predict a low annual CO outgas rate, $10^{-9} \text{ g cm}^{-2} \text{ s}^{-1}$; typically it should therefore be inactive, as is observed (Fornasier et al. 2014b). However, we argue that it should exhibit short CO outbursts, occurring twice an orbit after equinoxes and lasting of order a few months or longer. This would lift up the dust grains and be observed as a flaring in brightness or an excess in CO emission. Unfortunately, we know of no photometry of Chariklo after the last equinox in 2008 (Duffard et al. 2014), and the next one is not until 2039. For Chiron, two outbursts were reported in 1989 (Meech & Belton 1990) and 2001 (Romon-Martin et al. 2003; Jewitt 2009). While Ortiz et al. (2015) propose that Chiron was most likely at equinox in 1983 and 1999, Chariklo’s pole position is highly uncertain. Available lightcurves of Chiron are insufficient to allow a good pole solution (Person ???). Also, although the Ortiz et al. (2015) analysis is based on their interpretation of the Ruprecht et al. (2015) occultation data as rings, Ruprecht et al. (2015) themselves favor a jet/outburst interpretation. Nonetheless, if the Ortiz et al. (2015) equinox times are established firmly, they would indeed cast doubt on our model for ring formation at least for Chiron’s case and demand a new explanation for Chiron’s outbursts.

5. Summary

Assuming the width variations seen in Chariklo’s inner ring are long-lived, they indicate that the ring is apse-aligned, that its eccentricity changes by at least several parts in a thousand between its inner and outer edges, and, by analogy to the Uranian rings, that its overall eccentricity may be a few percent or more. If the apse alignment is maintained by a balance between self-gravity within the ring and Chariklo’s large J_2 moment, we find the total ring mass is of order a few $\times 10^{16}$ g. If the ring particles form a monolayer, they have typical size of order a few meters and velocity dispersion of order a few mm/s. These figures are a few times smaller than those observed in Saturn’s main rings (Zebker et al. 1985; French & Nicholson 2000) and are within the observational bounds for those of the ϵ ring of Uranus (French et al. 1991).

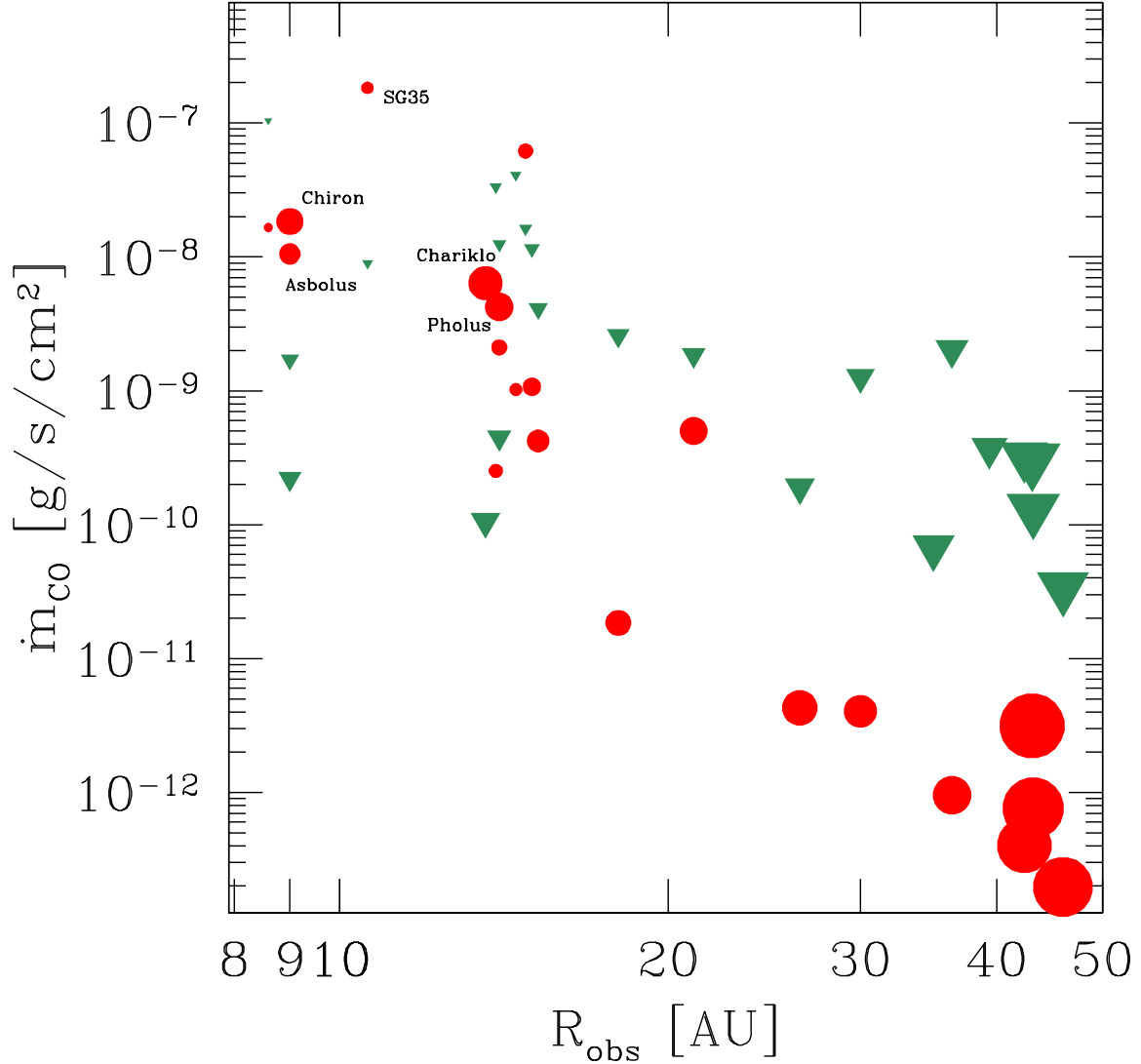


Fig. 3.— Per-area CO outgas rates vs. heliocentric distance at measurement dates for various Centaurs and KBOs. The upper limits (green down-ward pointing triangles) are taken from (Romon-Martin et al. 2003; Jewitt et al. 2008), and the theoretical rates (filled circles) are calculated using eq. 23, assuming a temperature that is appropriate for a blackbody receiving the orbit-averaged illumination, an albedo of $A = 0.05$, a porosity $\phi = 0.5$, a tortuosity $\tau = 2$, and a CO depletion depth of $\Delta\ell = 1$ km. The theoretical predictions are inconsistent with the observed upper limits for a few large Centaurs, marked by their respective names. This could reflect a longer (\gtrsim few Myr) residence time in the Centaur region. The symbol sizes indicate body sizes.

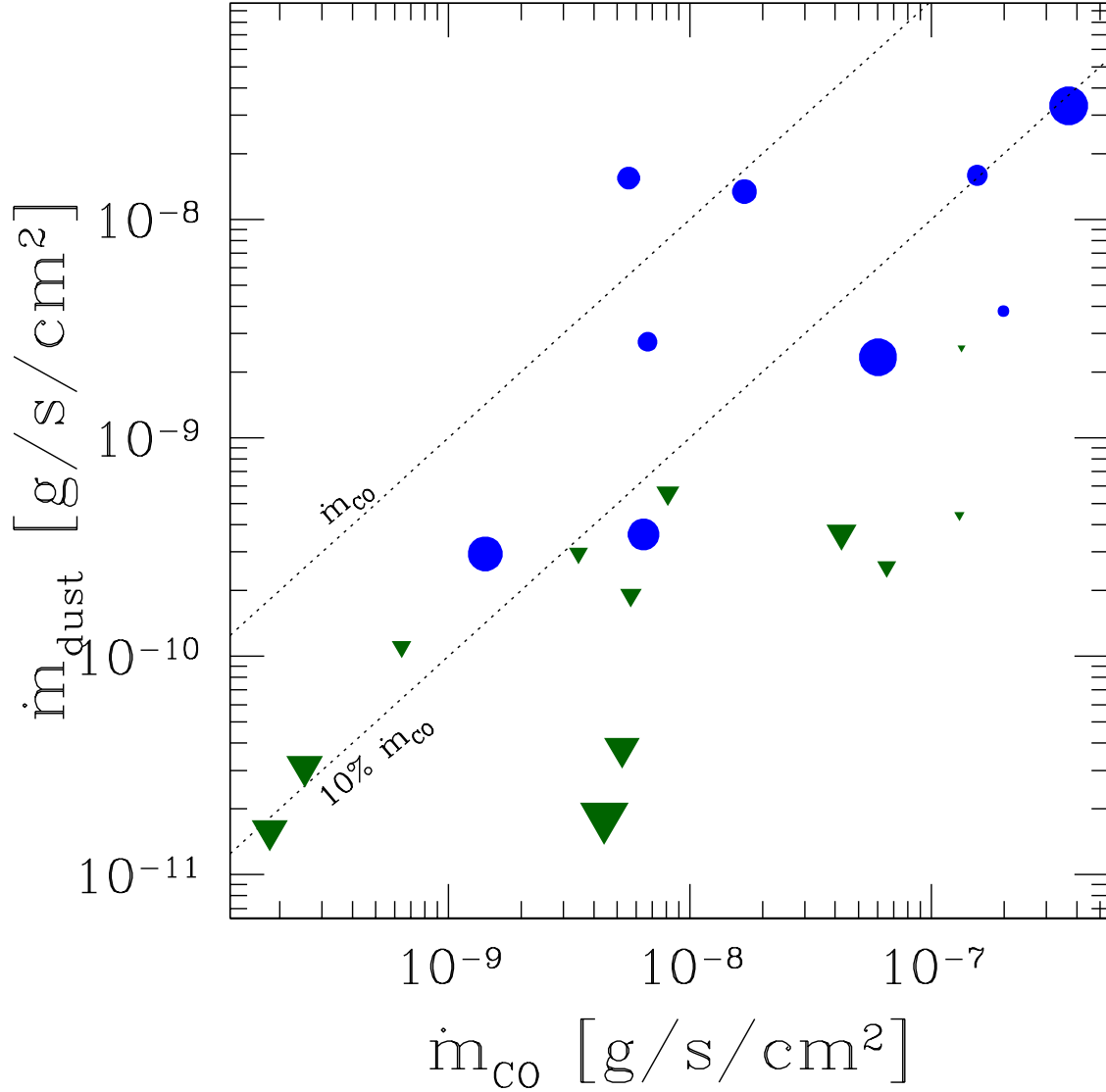


Fig. 4.— Observed dust production rate vs. predicted CO outgassing rate, with active Centaurs marked with filled circles and inactive ones marked as upper limits (Jewitt 2009). To obtain the dust production rate per unit area, we use estimated radii from Jewitt (2009). Particularly for active Centaurs the radii may be overestimated; this would tend to produce underestimates of the dust production per unit area. Consistent with Eq. (29), nearly all active objects have CO outgas rates above $\sim 10^{-8} \text{ g s}^{-1} \text{ cm}^{-2}$. Moreover, the dust production rate roughly scales with the predicted CO rate. Likewise, most inactive objects have CO outgas rates below $\sim 10^{-8} \text{ g s}^{-1} \text{ cm}^{-2}$; however, a few Centaurs with large predicted CO outgas rates remain inactive.

Our estimates of the ring particle size and velocity dispersion indicate that the ring’s collisional spreading time is of order 10^5 years, somewhat shorter than the typical Centaur dynamical lifetime of a few Myr (Bailey & Malhotra 2009). This short spreading time favors ring formation scenarios that occur during or after Chariklo’s move from the Kuiper belt to its current location among the giant planets. Thus, while impacts from ~ 10 km bodies during Chariklo’s few-Gyr sojourn in the Kuiper belt could easily have thrown enough ejecta into orbit to form rings, it is unlikely that rings so formed would have lasted long enough to be the ring system we see today. Perhaps more likely is ring formation from an initially close-in satellite pushed inside the Roche radius during the close encounter with Neptune that turned Chariklo into a Centaur. However, this requires a close match between the satellite’s initial orbit energy and the strength of the Neptune encounter. That 2060 Chiron likely also hosts rings (Duffard et al. 2014; Ortiz et al. 2015) suggests that Centaurs with rings may occur more often than this formation scenario can easily accommodate.

We also consider ring formation via a very different process: dust particles lifted from Chariklo into close orbit by an outflow of sublimated CO. When Chariklo shifted from a more distant orbit to one with its current ~ 16 AU periapse distance, the corresponding increase in the equilibrium temperature and therefore partial pressure of CO ~ 1 km below the surface could have forced dust particles off the surface and, after mutual collisions, into ring orbits. If rings are indeed associated with outgassing, we predict that they should be ubiquitous among large Centaurs but absent among small comets and very large KBOs (e.g., Pluto). In addition, our model predicts that the CO sublimation rate should surge within a few months of an equinox crossing. Further observations to refine the pole positions of Chariklo, Chiron, and possibly other Centaurs, and to monitor their brightness during the several months following equinoxes, would provide a very clear test for ring formation via outgassing.

Additional high-cadence and/or multi-chord occultation observations that further constrain the ring surface density profile, the ring widths, and Chariklo’s shape and orientation within the rings will help us better assess these and other formation mechanisms for the Chariklo system. Moreover, some of the proposed ring formation scenarios suggest that many more Centaurs should have rings or small moons. We hope that future occultation observations of different Centaurs can test this prediction.

We thank Maryame El Moutamid, Phil Nicholson, and an anonymous referee for knowledgeable and thought-provoking comments that led to improvements in this paper. We also acknowledge financial support by NSERC. MP thanks Bok Tower Gardens for their warm hospitality during the final stages of writing.

REFERENCES

Bailey, B. L., & Malhotra, R. 2009, *Icarus*, 203, 155

- Bieler, A., Altwegg, K., Balsiger, H., Bar-Nun, A., Berthelier, J.-J., Bochsler, P., Briois, C., Calmonte, U., Combi, M., de Keyser, J., van Dishoeck, E. F., Fiethe, B., Fuselier, S. A., Gasc, S., Gombosi, T. I., Hansen, K. C., Hässig, M., Jäckel, A., Kopp, E., Korth, A., Le Roy, L., Mall, U., Maggiolo, R., Marty, B., Mousis, O., Owen, T., Rème, H., Rubin, M., Sémon, T., Tzou, C.-Y., Waite, J. H., Walsh, C., & Wurz, P. 2015, *Nature*, 526, 678
- Biver, N., Bockelée-Morvan, D., Colom, P., Crovisier, J., Germain, B., Lellouch, E., Davies, J. K., Dent, W. R. F., Moreno, R., Paubert, G., Wink, J., Despois, D., Lis, D. C., Mehringer, D., Benford, D., Gardner, M., Phillips, T. G., Gunnarsson, M., Rickman, H., Winnberg, A., Bergman, P., Johansson, L. E. B., & Rauer, H. 1997, *Earth Moon and Planets*, 78, 5
- Bockelée-Morvan, D., Lellouch, E., Biver, N., Paubert, G., Bauer, J., Colom, P., & Lis, D. C. 2001, *A&A*, 377, 343
- Braga-Ribas, F., Sicardy, B., Ortiz, J. L., Snodgrass, C., Roques, F., Vieira-Martins, R., Camargo, J. I. B., Assafin, M., Duffard, R., Jehin, E., Pollock, J., Leiva, R., Emilio, M., Machado, D. I., Colazo, C., Lellouch, E., Skottfelt, J., Gillon, M., Ligier, N., Maquet, L., Benedetti-Rossi, G., Gomes, A. R., Kervella, P., Monteiro, H., Sfair, R., El Moutamid, M., Tancredi, G., Spagnotto, J., Maury, A., Morales, N., Gil-Hutton, R., Roland, S., Ceretta, A., Gu, S.-H., Wang, X.-B., Harpsøe, K., Rabus, M., Manfroid, J., Opitom, C., Vanzi, L., Mehret, L., Lorenzini, L., Schneiter, E. M., Melia, R., Lecacheux, J., Colas, F., Vachier, F., Widemann, T., Almenares, L., Sandness, R. G., Char, F., Perez, V., Lemos, P., Martinez, N., Jørgensen, U. G., Dominik, M., Roig, F., Reichart, D. E., Lacluyze, A. P., Haislip, J. B., Ivarsen, K. M., Moore, J. P., Frank, N. R., & Lambas, D. G. 2014, *Nature*, 508, 72
- Brown, M. E., van Dam, M. A., Bouchez, A. H., Le Mignant, D., Campbell, R. D., Chin, J. C. Y., Conrad, A., Hartman, S. K., Johansson, E. M., Lafon, R. E., Rabinowitz, D. L., Stomski, Jr., P. J., Summers, D. M., Trujillo, C. A., & Wizinowich, P. L. 2006, *ApJ*, 639, L43
- Brozović, M., Showalter, M. R., Jacobson, R. A., & Buie, M. W. 2015, *Icarus*, 246, 317
- Canup, R. M. 2004, *Icarus*, 168, 433
- Chiang, E. I., & Goldreich, P. 2000, *ApJ*, 540, 1084
- Clayton, J. O., & Giauque, W. F. 1932, *Journal of the American Chemical Society*, 54, 2610
- Cochran, A. L., Lvasseur-Regourd, A.-C., Cordiner, M., Hadamcik, E., Lasue, J., Gicquel, A., Schleicher, D. G., Charnley, S. B., Mumma, M. J., Paganini, L., Bockelée-Morvan, D., Biver, N., & Kuan, Y.-J. 2015, *Space Sci. Rev.*
- Cowan, J. J., & Ahearn, M. F. 1982, *Icarus*, 50, 53
- Crovisier, J., Biver, N., Bockelee-Morvan, D., Colom, P., Jorda, L., Lellouch, E., Paubert, G., & Despois, D. 1995, *Icarus*, 115, 213

- Cuzzi, J., Clark, R., Filacchione, G., French, R., Johnson, R., Marouf, E., & Spilker, L. 2009, Ring Particle Composition and Size Distribution, ed. Dougherty, M. K., Esposito, L. W., & Krimigis, S. M., 459–+
- De Sanctis, M. C., Capaccioni, F., Ciarniello, M., Filacchione, G., Formisano, M., Mottola, S., Raponi, A., Tosi, F., Bockelée-Morvan, D., Erard, S., Leyrat, C., Schmitt, B., Ammannito, E., Arnold, G., Barucci, M. A., Combi, M., Capria, M. T., Cerroni, P., Ip, W.-H., Kuehrt, E., McCord, T. B., Palomba, E., Beck, P., Quirico, E., VIRTIS Team, Piccioni, G., Bellucci, G., Fulchignoni, M., Jaumann, R., Stephan, K., Longobardo, A., Mennella, V., Migliorini, A., Benkhoff, J., Bibring, J. P., Blanco, A., Blecka, M., Carlson, R., Carsenty, U., Colangeli, L., Combes, M., Crovisier, J., Drossart, P., Encrenaz, T., Federico, C., Fink, U., Fonti, S., Irwin, P., Langevin, Y., Magni, G., Moroz, L., Orofino, V., Schade, U., Taylor, F., Tiphene, D., Tozzi, G. P., Biver, N., Bonal, L., Combe, J.-P., Despan, D., Flamini, E., Fornasier, S., Frigeri, A., Grassi, D., Gudipati, M. S., Mancarella, F., Markus, K., Merlin, F., Orosei, R., Rinaldi, G., Cartacci, M., Cicchetti, A., Giuppi, S., Hello, Y., Henry, F., Jacquino, S., Rees, J. M., Noschese, R., Politi, R., & Peter, G. 2015, *Nature*, 525, 500
- De Sanctis, M. C., Capria, M. T., & Coradini, A. 2001, *AJ*, 121, 2792
- De Sanctis, M. C., Capria, M. T., Coradini, A., & Orosei, R. 2000, *AJ*, 120, 1571
- Descamps, P., & Marchis, F. 2008, *Icarus*, 193, 74
- Donn, B. 1963, *Icarus*, 2, 396
- Duffard, R., Pinilla-Alonso, N., Ortiz, J. L., Alvarez-Candal, A., Sicardy, B., Santos-Sanz, P., Morales, N., Colazo, C., Fernández-Valenzuela, E., & Braga-Ribas, F. 2014, *A&A*, 568, A79
- El Moutamid, M. 2014, private communication
- Enzian, A., Cabot, H., & Klinger, J. 1997, *A&A*, 319, 995
- Evans, R. B., Watson, G. M., & Mason, E. A. 1961, *J. Chem. Phys.*, 35, 2076
- Fornasier, S., Lazzaro, D., Alvarez-Candal, A., Snodgrass, C., Tozzi, G. P., Carvano, J. M., Jiménez-Teja, Y., Silva, J. S., & Bramich, D. M. 2014a, *A&A*, 568, L11
- . 2014b, *A&A*, 568, L11
- French, R. G., & Nicholson, P. D. 2000, *Icarus*, 145, 502
- French, R. G., Nicholson, P. D., Porco, C. C., & Marouf, E. A. 1991, Dynamics and structure of the Uranian rings, ed. J. T. Bergstrahl, E. D. Miner, & M. S. Matthews, 327–409
- Goldreich, P., Lithwick, Y., & Sari, R. 2002, *Nature*, 420, 643
- Goldreich, P., & Tremaine, S. 1979a, *AJ*, 84, 1638

—. 1979b, *Nature*, 277, 97

Grundy, W. M., Porter, S. B., Benecchi, S. D., Roe, H. G., Noll, K. S., Trujillo, C. A., Thirouin, A., Stansberry, J. A., Barker, E., & Levison, H. F. 2015, *Icarus*, 257, 130

Guilbert-Lepoutre, A. 2011, *AJ*, 141, 103

Gunnarsson, M., Rickman, H., Festou, M. C., Winnberg, A., & Tancredi, G. 2002, *Icarus*, 157, 309

Jewitt, D. 2009, *AJ*, 137, 4296

Jewitt, D., Garland, C. A., & Aussel, H. 2008, *AJ*, 135, 400

Klinger, J. 1980, *Science*, 209, 271

Kochan, H., Feuerbacher, B., Joo, F., Klinger, J., Seboldt, W., Bischoff, A., Duren, H., Stoffler, D., Spohn, T., Fechtig, H., Grun, E., Kohl, H., Krankowsky, D., Roessler, K., Thiel, K., Schwehm, G., & Weishaupt, U. 1989, *Advances in Space Research*, 9, 113

Leinhardt, Z. M., & Stewart, S. T. 2012, *ApJ*, 745, 79

Meech, K. J., & Belton, M. J. S. 1990, *AJ*, 100, 1323

Murray, C. D., & Dermott, S. F. 1999, *Solar system dynamics*

Nicholson, P. D., Persson, S. E., Matthews, K., Goldreich, P., & Neugebauer, G. 1978, *AJ*, 83, 1240

Noll, K. S., Grundy, W. M., Chiang, E. I., Margot, J.-L., & Kern, S. D. 2008, *Binaries in the Kuiper Belt*, ed. M. A. Barucci, H. Boehnhardt, D. P. Cruikshank, A. Morbidelli, & R. Dotson, 345–363

Ortiz, J. L., Duffard, R., Pinilla-Alonso, N., Alvarez-Candal, A., Santos-Sanz, P., Morales, N., Fernández-Valenzuela, E., Licandro, J., Campo Bagatin, A., & Thirouin, A. 2015, *ArXiv e-prints*

Ortiz, J. L., Thirouin, A., Campo Bagatin, A., Duffard, R., Licandro, J., Richardson, D. C., Santos-Sanz, P., Morales, N., & Benavidez, P. G. 2012, *MNRAS*, 419, 2315

Person. ????

Pravec, P., Vokrouhlický, D., Polishook, D., Scheeres, D. J., Harris, A. W., Galád, A., Vaduvescu, O., Pozo, F., Barr, A., Longa, P., Vachier, F., Colas, F., Pray, D. P., Pollock, J., Reichart, D., Ivarsen, K., Haislip, J., Lacluyze, A., Kušnirák, P., Henych, T., Marchis, F., Macomber, B., Jacobson, S. A., Krugly, Y. N., Sergeev, A. V., & Leroy, A. 2010, *Nature*, 466, 1085

Prialnik, D., & Bar-Nun, A. 1987, *ApJ*, 313, 893

Prialnik, D., Brosch, N., & Ianovici, D. 1995, *MNRAS*, 276, 1148

- Ragozzine, D., & Brown, M. E. 2009, *AJ*, 137, 4766
- Rauer, H., Biver, N., Crovisier, J., Bockelée-Morvan, D., Colom, P., Despois, D., Ip, W.-H., Jorda, L., Lellouch, E., Paubert, G., & Thomas, N. 1997, *Planet. Space Sci.*, 45, 799
- Romon-Martin, J., Delahodde, C., Barucci, M. A., de Bergh, C., & Peixinho, N. 2003, *A&A*, 400, 369
- Rubin, M., Altwegg, K., Balsiger, H., Bar-Nun, A., Berthelier, J.-J., Bieler, A., Bochsler, P., Briois, C., Calmonte, U., Combi, M., De Keyser, J., Dhooghe, F., Eberhardt, P., Fiethe, B., Fuselier, S. A., Gasc, S., Gombosi, T. I., Hansen, K. C., Hässig, M., Jäckel, A., Kopp, E., Korth, A., Le Roy, L., Mall, U., Marty, B., Mousis, O., Owen, T., Rème, H., Sémon, T., Tzou, C.-Y., Waite, J. H., & Wurz, P. 2015a, *Science*, 348, 232
- Rubin, M., Altwegg, K., van Dishoeck, E. F., & Schwehm, G. 2015b, *ArXiv e-prints*
- Ruprecht, J. D., Bosh, A. S., Person, M. J., Bianco, F. B., Fulton, B. J., Gulbis, A. A. S., Bus, S. J., & Zangari, A. M. 2015, *Icarus*, 252, 271
- Schlichting, H. E., Ofek, E. O., Sari, R., Nelan, E. P., Gal-Yam, A., Wenz, M., Muirhead, P., Javanfar, N., & Livio, M. 2012, *ApJ*, 761, 150
- Senay, M. C., & Jewitt, D. 1994, *Nature*, 371, 229
- Sicardy, B., Braga-Ribas, F., Ortiz, J. L., Vieira-Martins, R., Colas, F., Duffard, R., Camargo, J. I., Desmars, J., Gulbis, A., Assafin, M., Maquet, L., Beisker, W., Benedetti-Rossi, G., Vachier, F., Dumas, C., Ivanov, V. D., Renner, S., Bath, K.-L., Klotz, A., Pollock, J. T., Lecacheux, J., Dauvergne, J.-L., Peyrot, A., & Teng, J.-P. 2014, in *AAS/Division for Planetary Sciences Meeting Abstracts*, Vol. 46, *AAS/Division for Planetary Sciences Meeting Abstracts*, 408.01
- Stewart, S. T., & Leinhardt, Z. M. 2009, *ApJ*, 691, L133
- Whipple, F. L. 1989, *ApJ*, 341, 1
- Womack, M., & Stern, S. A. 1997, in *Lunar and Planetary Science Conference*, Vol. 28, *Lunar and Planetary Science Conference*, 1575
- Zebker, H. A., Marouf, E. A., & Tyler, G. L. 1985, *Icarus*, 64, 531